

4 FEL Physics

Synopsis

The FERMI@Elettra project is based on the harmonic up-shifting of an initial “seed” signal in a single-pass FEL amplifier employing multiple undulators. The basic principles which underlie this approach are: the energy modulation of the electron beam via the resonant interaction with an external laser seed in a first undulator (modulator); the use of a chromatic dispersive section to then develop a strong density modulation with large harmonic overtones; the production of coherent radiation by the microbunched beam in a downstream undulator (radiator). The first stage of the project, FEL-1, will generate coherent output radiation in the 40-100 nm spectral range. For these wavelengths, users require short (<100 fs) pulses with adjustable polarization and high temporal and spatial reproducibility. FEL-1 relies upon a single-stage, harmonic generation scheme (i.e., modulator-dispersive section-radiator), like the one already operational at Brookhaven [1,2].

The project’s second stage, FEL-2, extends the spectral range to 10 nm. Present user requirements include narrow-bandwidth pulses with high peak brilliance and adjustable polarization. For FEL-2, a two-stage harmonic cascade is needed to reach short wavelengths. The selected configuration is based on the so-called “fresh bunch” approach [3], in which the output from the first radiator energy modulates (in a subsequent modulator) a part of the electron beam that did not interact with the external seed. If at the time FEL-1 becomes operational a suitable seed laser source (using harmonic generation in gas) is available at ~ 40 nm, then FEL-2 could be operate with a single up-shift in frequency as in FEL-1 thus eliminating the harmonic cascade. Design choices for FEL-2 do not preclude this attractive possibility.

For the first modulator, which must satisfy FEL resonance over a nominal wavelength range of 240 to 360 nm, the undulator wavelength, λ_w , selected is 160 mm. For the second stage modulator of FEL-2, the adopted λ_w is 65 mm, matching that of the first stage radiator. The choice of λ_w for the radiators is driven by two principal requirements: (1) the FEL resonance be physically possible at the maximum output wavelength (*i.e.*, 100 nm for FEL-1 and 40 nm for FEL-2) for beam energies of 1.2 GeV; (2) there be sufficient gain (*i.e.*, $a_w \geq 1$, a_w being the normalized rms undulator magnetic strength) at the shortest desired output wavelength. To deliver output radiation with a polarization that is continuously tunable from linear to circular polarizations, the final radiators have an APPLE configuration. Wavelength tuning will be done by changing the undulator gap (and thus a_w) rather than by changing the electron beam energy. As the coupling between the radiation and the electron beam can depend strongly upon beam radius, the FERMI design includes external quadrupole focusing to produce an average value of 10 m for the Twiss beta function in each plane.

Of major concern are variations in beam characteristics affect the shot-to-shot repeatability of the FEL output. The most sensitive parameter is the initial electron beam energy. A critical quantity affecting the requisite electron beam duration is the timing jitter of the beam relative to that of the seed laser. An electron beam pulse of at least 600 fs is needed for 100 fs seed pulses. This timing jitter is one of the most demanding requirements on the injector and accelerator subsystems.

Adopting slightly off-optimum parameters (with respect to output power) lessens the sensitivity of the FEL performance. As the final design of FEL-2 will be modified based on FEL-1 performance, present calculations are representative rather than fully consistent design sets. For both FEL-1 and FEL-2, calculations based on time-steady input parameters and full start-to-end time-dependent simulations were performed using the 3D numerical codes Genesis [4] and Ginger [5]. Wakefields from surface roughness of the beam pipe in the undulator are seen to yield values that are much smaller than the fundamental FEL parameter and much smaller than the energy jitter from all sources (~0.09%). Consequently this phenomenon should have minimal effect on the output power or effective bandwidth of the FELs.

4.1 Introduction

The FERMI@Elettra project is based on the principle of harmonic up-conversion of an initial “seed” signal in a single pass, FEL amplifier employing multiple undulators. The basic principles which underlie this approach to obtaining short wavelength output are: the energy modulation of the electron beam via the resonant interaction with an external laser seed in a first undulator (called “modulator”); the use of a chromatic dispersive section to then develop a strong density modulation with large harmonic overtones; the production of coherent radiation by the micro-bunched beam in a downstream undulator (called “radiator”). In the following, each of these elements is discussed in turn.

An external laser provides an initial, wavelength-tunable seed signal. This signal, in conjunction with the magnetic field generated by the modulator, produces a relatively strong energy modulation $\Delta\gamma$ of the beam electrons via resonant interaction. The modulation has a sinusoidal variation in time identical to that of the seed’s angular frequency, $\omega_0 (=2\pi c/\lambda_0$, where λ_0 is the seed wavelength). When the modulator’s length is comparable to or shorter than the exponential gain length for FEL radiation power *and* when the number of undulator periods obeys the relation $2N_u (\Delta\gamma/\gamma_0) < 1$, very little accompanying density modulation (*i.e.*, micro-bunching) is produced in the modulator.

Following its exit from the modulator, the electron beam then passes through a chromatic dispersion section in which a density modulation develops from path length differences associated with the energy modulation. So long as $\Delta\gamma \gg \sigma_\gamma$, where σ_γ is the initial “incoherent” slice energy spread, a strong periodic density modulation is created at wavelength λ_0 containing large higher harmonic components (up to harmonic number $m \sim \Delta\gamma / \sigma_\gamma$). Note that at a given longitudinal position in the electron beam, the relative spread in the induced $\Delta\gamma$ must also be quite small or else the density modulation will be degraded, especially at higher harmonics. Consequently, the transverse extent of the seed laser (assumed to be characterized by a Gaussian-like transverse profile) should be significantly greater than that of the electron beam.

At this point the electron beam enters the radiator, whose wavelength and magnetic strength are tuned such that the FEL resonance occurs at an integral harmonic m of the original seed laser wavelength:

$$\lambda_R = \frac{\lambda_0}{m} = \frac{\lambda_u}{2\gamma^2} (1 + a_w^2) \quad 4.1.1$$

where a_w is the normalized rms undulator magnetic strength. For FERMI, m varies between 3 and 6 for the first radiator. If, as in FEL-1, this radiator is the final undulator, it generally is made sufficiently long for the FEL radiation to grow to saturation (or even longer via tapering if greater output power is sought).

For a multistage harmonic cascade such as FEL-2, the first radiator is generally much shorter than that necessary for power saturation. In the so-called “fresh bunch” approach, the duration of the electron bunch is several times longer than the duration of the seed laser pulse. In that case radiation from the first radiator is used to energy-modulate part of the electron beam in a subsequent modulator, the first radiator is made only long enough that the radiation is sufficient to produce adequate downstream energy modulation. The emitted radiation is effectively coherent spontaneous emission, whose power scales as the square of the product of the current and the longitudinal distance inside the undulator (ignoring diffraction and debunching effects). Following the first radiator is a section (essentially a chicane) that temporally delays the electron beam in order to make the output radiation temporally coincident with a “fresh” section of the electron beam closer to the beam head. This fresh section of the bunch has not had its incoherent energy spread increased via FEL interaction in the first stage modulator and radiator. Thus, it can be far more easily energy- and density-modulated in the second stage undulators than the “used” electron beam section that interacted with the seed laser pulse in the first modulator and radiator.

The second stage for the fresh bunch approach consists of a modulator, a final radiator, and, in general, an intervening dispersive section. The modulator uses the radiation from the first stage radiator as its seed radiation; it must therefore have its undulator period and magnetic strength tuned to be resonant at that same wavelength. Since the radiation diffracts freely once it departs the first radiator, care must be taken 1) that the temporal delay section is not too long and 2) that the necessary second modulator length does not exceed the Rayleigh length. Otherwise, the coupling between the radiation and the electron beam may be too weak for sufficient energy modulation to develop. The second stage modulator, radiator, and intervening dispersive section are quite similar in concept to the first stage. In general, the harmonic upshift factor between the second stage modulator and radiator is 4 or less for the FERMI case. Moreover, the amount of microbunching at the new harmonic in the second radiator is also generally less than half that produced in the first stage because both the undulator parameter a_w and the initial radiation intensity are smaller.

This combination generally leads to a smaller energy modulation at the end of the second modulator. The second stage radiator is usually much longer than that of the first stage both because the initial bunching is normally smaller and because the FEL is normally run to saturation (which requires more distance because the corresponding exponential gain lengths are longer due to the smaller a_w). The process of light emission in the final radiator includes at first quadratic part (as in the first stage and in single-stage FEL-1 configuration) and then an exponential growth regime. This it is similar to the classic HGHG scheme of Yu.

4.2 Basic FEL Output Requirements and Related Issues

The baseline FEL output requirements for FEL-1 and FEL-2 are summarized in Table 4.2.1. At all wavelengths, both FEL-1 and FEL-2 are to have continuously tunable output polarization ranging from linear-horizontal to circular to linear-vertical. Consequently, the FEL-1 radiator and final radiator in FEL-2 have an APPLE configuration. Both FELs will operate at 10-50 Hz; this specification is constrained by the accelerator (see chapter 6) and not by the FEL subsystems.

Present scientific proposals for the application of FEL-1 involve time-domain experiments such as pump-probe interactions and possibly nonlinear phenomena. Consequently, the requirements for FEL-1 are more related to total photon number per pulse (*i.e.*, $0.4 - 2 \times 10^{14}$) and pulse duration (20-100 fs) than they are to spectral bandwidth. A critical parameter affecting the requisite electron beam duration is the timing jitter of the beam relative to that of the seed laser. In order to assure sufficient overlap between the seed and the electrons, the duration of the electron bunch must be longer than the duration of the seed pulse plus two times the rms timing jitter. If the expected rms timing jitter from the accelerator is of order 150 fs (see Chapter 6), an electron bunch duration of at least 600 fs is needed for 100 fs seed pulses. This timing jitter is one of the most demanding requirements on the injector and accelerator subsystems.

Another important parameter associated with FEL-1 time domain experiments is shot-to-shot repeatability. Ideally, for nonlinear phenomena experiments, the shot-to-shot rms jitter in normalized photon number should be 5% or less. As explained in Section 4.4, such a low value seems unlikely with the presently expected accelerator and injector parameters. A large class of FEL-1 experiments can tolerate values as high as 25% by recording the shot-by-shot photon number for post-processing. Other FEL-1 output specifications related to jitter parameters are: pointing, virtual waist location and angular divergence jitter, shot-to-shot transverse profile changes. Although none of these is likely on an individual basis to prevent FERMI from successfully reaching the goal of 5% (spatially) local intensity fluctuations at the experimental sample, taken together they will likely produce jitter exceeding this goal even in the absence of fluctuations in photon number. Notably, some experiments (*e.g.*, those using gaseous samples) may be insensitive to pointing or profile changes. In the operation of FEL-1, the wavelength jitter should be less than the individual shot bandwidth in order to not increase the effective time-averaged, output bandwidth as seen by the user.

In contrast to FEL-1, in which timing and photon number jitter are critical parameters, most FEL-2 users are (presently) interested in frequency domain experiments in which longitudinal coherence and narrow bandwidth are most important. The most important output goal for FEL-2 is $\geq 10^{12}$ photons/pulse/meV. Consequently, FEL-2 specifications favour long output pulses (≥ 1 ps) whose spectral properties ($\Delta E_\omega < 10$ meV) are as close as possible to the transform limit. Although the total photon jitter is not critical for most experiments in the frequency domain, shot-to-shot central wavelength jitter during

Table 4.2.1: FEL-1 and FEL-2 expected performance.

<i>Parameter</i>	<i>FEL-1</i>	<i>FEL-2</i>
Wavelength range [nm]	100 to 40	40 to 10
Output pulse length (rms) [fs]	≤ 100	> 200
Bandwidth (rms) [meV]	17 (at 40 nm)	5 (at 10 nm)
Polarization	Variable	Variable
Repetition rate [Hz]	50	50
Peak power [GW]	1 to >5	0.5 to 1
Harmonic peak power (% of fundamental)	~ 2	~ 0.2 (at 10 nm)
Photons per pulse	10^{14} (at 40 nm)	10^{12} (at 10 nm)
Pulse-to-pulse stability	$\leq 30\%$	$\sim 50\%$
Pointing stability [μ rad]	< 20	< 20
Virtual waist size [μ m]	250 (at 40 nm)	120
Divergence (rms, intensity) [μ rad]	50 (at 40 nm)	15 (at 10 nm)

narrow bandwidth operation may be of concern unless the bandwidth can be maintained at or below the required spectral resolution (~ 5 meV).

For some experiments (such as RIXS where one is examining a small inelastic scattering cross-section in the presence of a much larger elastic scattering cross-section), a spectral resolution of 10^5 requires that the integrated noise photon level (at the detector) be less than 1 part in 10^5 of the wanted signal. Without spectral filtering, this requirement could be more severe than that of rms bandwidth. For example, if the integrated noise power is 1 part in 10^4 but has a bandwidth 100 times greater than the main signal, the total (signal + noise) rms bandwidth increases by only $\sim 40\%$ from that of the signal, but the unfiltered spectral resolution would still miss the 10^5 criterion by a factor of ten.

A multi-stage harmonic cascade is more sensitive to energy spread than SASE because of the very non-linear process leading to harmonic micro-bunching at the seed frequency. A very sharp limit in fact exists on the tolerable bunch energy spread.

Furthermore, because in multi-stage operation the first stage output radiation power scales quadratically with bunch current, the end output power also drops sharply as the bunch current is lowered below design. Should one rely upon strong exponential gain in the final radiator the output power would also be very sensitive to the beam current.

4.3 Undulator and Transport Lattice Design

4.3.1 Choice of Undulator Type and Wavelength

Due to the requirement that the output radiation polarization be continuously tunable from linear to circular, the FERMI project has chosen the APPLE configuration for the final radiators (FEL-1 radiator and FEL-2 second stage radiator). For the initial modulator, a simple, linearly-polarized configuration is optimal both due to its simplicity and because the input radiation seed can be linearly polarized. As the short first modulator produces little if any gain, there is little cost or space advantage in using a circular polarization for which the electron beam/radiation coupling is somewhat better. For the case of the first stage radiator and second stage modulator (for the fresh bunch approach), FEL-2, will use linearly-polarized undulators, because of their simplicity and lower cost. If for whatever reasons (*e.g.*, suppression of higher harmonic emission) circular polarization is required, such a design change could be made without requiring greater undulator length.

Wavelength tuning in the undulators will be done by changing the gap (and thus a_w) rather than by changing the electron beam energy. Hence, the maximum wavelength reachable for a given fixed beam energy is set by the magnetic field at the undulator pole tips, the minimum gap obtainable, and the undulator wavelength. These considerations strongly constrain the available parameter space, especially for FEL-1.

For the first modulator, which must satisfy FEL resonance over a nominal wavelength range of 240 to 360 nm, the undulator wavelength selected is 160 mm. For the second stage modulator of FEL-2, the adopted undulator wavelength of 65 mm agrees with that chosen for the first stage radiator (see the discussion in the next paragraph). The choice of undulator wavelength for the radiators is driven by two principal requirements: (1) the FEL resonance be physically possible at the longest desired output wavelength (*i.e.*, 100 nm for FEL-1 and 40 nm for FEL-2) at an electron beam energy of 1.2 GeV; (2) there be reasonable gain (*i.e.*, $a_w \geq 1$) at the shortest desired output wavelength. The first requirement drives one to small gaps (for large a_w) and longer wavelengths. The second requirement pushes one to shorter wavelengths (but as λ_u decreases, the maximum possible a_w for a given gap opening begins to decrease exponentially making the first requirement becomes difficult to meet). The present design choice is a minimum gap opening of 10 mm; this value allows for an 8 mm “stay clear”, a 1 mm pipe thickness, and 1 mm clearance. With all this in mind, a 65 mm wavelength was chosen for the FEL-1 radiator and first FEL-2 radiator and a 50 mm wavelength for the final FEL-2 radiator.

4.3.2 Undulator Segmentation and Focusing Issues

In order to produce high powers, the active radiator lengths for FEL-1 and FEL-2 are in the range 15-30 m – far too long to be practical as one continuous magnetic structure. Consequently, the radiators will be subdivided into modules, each consisting of an active segment of undulator and a drift section with containing elements such as quadrupoles, a longitudinal phase shifter, beam position monitors, dipole correctors, and diagnostics. Tentatively, ~ 1.0 m is allowed for the end drift sections; the exact distance will be determined on the basis of detailed engineering. In order to keep the fraction of space occupied by the active magnetic segment reasonable (*i.e.*, ≥ 0.5), lengths of 2.34 m (= 36 periods) for the FEL-1 and first FEL-2 radiators, and 2.40 m (= 48 periods) for the second FEL-2 radiator have been chosen. These “active”, full strength lengths do not include the 2-3 poles at the beginning and end of each segment of

undulator needed for adiabatic matching. While longer undulator segments are permitted by magnetic force considerations, the desire for a Twiss beta function of $\sim 7\text{-}10$ m limits the total module length to ~ 3.5 m.

The coupling between the radiation and the electron beam can depend strongly upon the beam radius. As the FEL radiation emissivity scales directly with the electron beam density, there is a premium for minimizing the beam radius. However, reducing the electron beam radius increases the spread of transverse velocities (due to emittance). Diffraction (which spreads the radiation) can reduce the coupling despite the larger current density. Consequently, for a given emittance and radiation wavelength, there is an optimum electron beam radius for maximizing energy extraction. For FERMI, this radius is generally in the vicinity of 100 microns. For normalized electron beam emittance of ~ 1.5 mm-mrad, this radius is much smaller than that obtainable with the natural focusing of the undulator. Consequently, our design includes external quadrupole focusing to produce an average value of 10 m for the Twiss beta function in each plane.

The external quadrupoles also compensate for changes in natural undulator focusing 1) since a_w is being changed when varying the output wavelength, and 2) at a fixed wavelength, whenever the undulator polarization is changed (e.g., from vertical to circular). For APPLE-type undulators the focusing for circular and vertical polarization can be negative (i.e., defocusing) in the x -plane; for long undulators such as the final radiator in FEL-2, this defocusing must be compensated for by external focusing. Thus, the FERMI control system must actively modify the quadrupole strengths whenever non-negligible changes are made in the undulator gaps and/or polarizations.

The decision to tune output wavelengths by changing the undulator gaps (i.e., a_w values) implies active control of the longitudinal phase slip between the electron beam and radiation in the drifts between undulator sections. The phase advance in a simple drift section of length L_B , $\Delta\theta = k_w L_B / (1 + a_w^2)$, is not necessarily a multiple of 2π as one varies the FEL wavelength λ_s (and thus a_w). Consequently, a very weak magnetic chicane (strength $R_{s6} \sim 2\lambda_s$) is needed to act as a “phase shifter” in the drift section. The initial estimate is that that ~ 200 mm of longitudinal space will be needed for this element.

4.3.3 Undulator Error Tolerance Calculation

Apart from electron beam errors such as offset, tilt, and mismatch, other errors are possible within the undulator. These include: 1) tilt and offsets of entire segments of undulator, 2) “global” segment mistuning errors such that the average a_w is offset by a constant amount within each segment (e.g. due to an incorrect gap setting), 3) “local” undulator errors due to individual pole strength errors. Local errors can lead both to longitudinal phase errors between the electron beam and the FEL radiation and to the electron beam wandering away from the central axis of undulator and radiation.

To lowest order, tilt and offset in the undulator are equivalent to errors (equal and opposite in value) in the initial electron beam position and tilt. Sensitivity to such errors is discussed in Section 4.4.2. In a multi-segment undulator, the effect of these errors could, in a statistical sense, grow as \sqrt{N} where N is the number of segments. Hence, if the overall tolerable tilt and offset values are, say, Y , then the equivalent rms tolerances on individual segments might need to be reduced to Y/\sqrt{N} . However, with active dipole correctors between segments this estimate may be unduly pessimistic.

“Global” mistuning of segments will lead to a longitudinal phase error that grows with distance along the undulator. If this error becomes comparable to $\pi/2$ radians, there can be significant loss of FEL gain.

In contrast, smaller scale errors in some circumstances can lead to higher radiation power than obtainable from a constant a_w undulator. This effect appears due to a serendipitous tapering which extracts more power. A rough criterion for the rms accuracy of setting a_w (equivalently the gap opening) in the FEL-1 radiator and the final radiator of FEL-2, was obtained from a series of GINGER runs in which random mistunings with a given rms expectation value were applied to each individual radiator segment. For FEL-1 at 40-nm output wavelength, the results (see Figure 4.3.1 left) show that on average, the rms segment mistuning error in a_w must exceed 0.002 before the output power begins to drop more than a few percent. This constraint appears to be relatively easy to meet for the FERMI undulators. For FEL-2, the results (see Figure 4.3.1 right) are quite similar with rms errors below 0.002 showing essentially no effect on the average output power at 10-nm with the standard deviation remaining less than 10%.

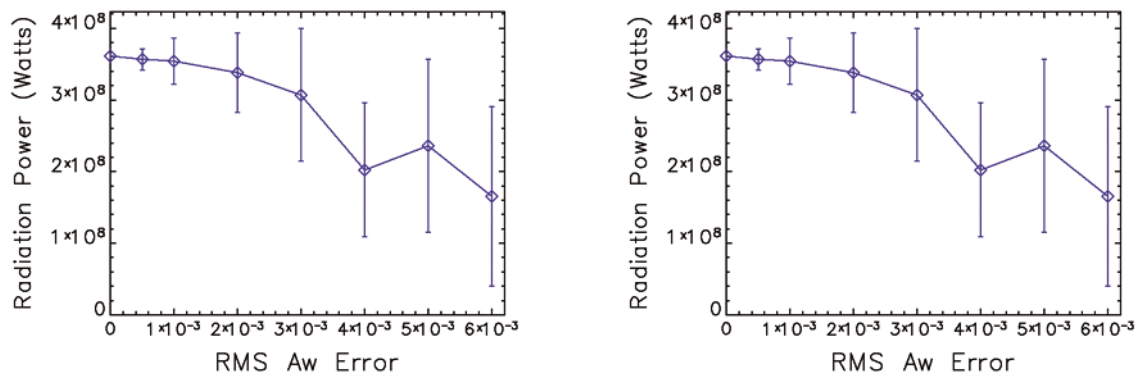


Figure 4.3.1:

Left: Output radiation power at 40-nm from FEL-1 in the presence of random segment of undulator mistuning as a function of rms error in a_w . The diamond symbol and error bars refer to the mean and standard deviation

over 64 independent mistunings. The distribution of errors at individual segments follows a one-dimensional Gaussian. Right: Output radiation power at 10-nm from FEL-2 (fresh bunch approach). The diamond symbol

and error bars refer to the mean and standard deviation over 25 independent mistunings. The distribution of errors at individual segments follows a one-dimensional Gaussian.

Within each undulator period, the two individual pole errors of one undulator period are decomposed into an “even” component which leads to no net transverse kick but does induce a phase error through a net change in a_w , and an “odd” component that produces a net transverse kick on the beam. This odd component causes the electron beam both to wander off-axis and also to suffer a net phase error. In the absence of any correction, the beam-wander increases steadily with z , as does the longitudinal phase error.

In the actual physical situation, for a given sorting of the individual poles within a given segment of undulator, the strength errors are “frozen” (i.e., do not vary in time) and may therefore be corrected in an average sense in z by the insertion of dipole shims. With “virtual” shims implemented in the XWIGERR code, time independent GINGER calculations were performed to determine output power sensitivity to undulator pole strength errors for FEL-1 at 40-nm and FEL-2 at 10-nm (fresh bunch approach) [3].

Results show a relatively tight correlation between the residual phase error and the output power. For FEL-1, virtually no power is lost for residual phase errors below 0.2 radians; for FEL-2 at 10-nm the equivalent value is 0.15 radians. The correlations are less for tilt and offset residuals. For FEL-1, little power is lost for <20-micron offsets and 50-microradian tilts; for FEL-2 the equivalent numbers are ~10 microns and 25 microradians. These values constitute system requirements for the FEL undulator.

4.3.4 Post-Modulator Dispersive Section Design and Issues

Following each modulator a dispersive magnetic chicane produces a strong coherent micro-bunching from the energy modulation impressed upon the electron beam by the FEL interaction in the modulator. For reasonably large input seed powers (e.g. ≥ 10 MW) and short wavelengths ($\lambda_0 \leq 300$ nm), the necessary R_{56} dispersion parameter is ~ 100 μm or less in the first stage modulator. For the fresh bunch approach, the second stage dispersive element is typically 5 times smaller. Preliminary design of the dispersive sections reveals no significant engineering or space issues. Detailed analysis is still required to set limits for higher order optical terms, such as could be induced by fringe fields and/or geometric aberrations. However, no practical problems are expected given the allowed longitudinal space of ~ 30 m and the relatively large seed wavelength. The actual design of the dipole elements of this chicane could introduce a transverse focusing effect that will be properly modelled with the FEL simulation codes.

4.3.5 Delay Section Needs and Issues for FEL-2 Fresh-Bunch Approach

In the fresh bunch approach to FEL-2, the e-beam must be delayed by $\sim 0.5 - 1.0$ ps relative to the FEL radiation in order that a “fresh” section of the e-beam be energy-modulated in the second stage modulator. A 1-ps delay is equivalent to an R_{56} of 600 μm . Inasmuch as the radiation field carries the “imprinting” signal, the allowed longitudinal space of ~ 1.8 m is more than adequate to contain the needed chicane. The delay section must also contain various diagnostics and at least a quadrupole singlet (and possibly doublet) for matching the e-beam to the second stage optics. FEL simulations of this section include diffractive effects.

4.4 FEL-1 Design and Parameters Calculations

The nominal design parameters of FEL-1 are presented in Table 4.4.1.

Table 4.4.1: Nominal design value and presumed rms jitter for FEL-1 parameter.

<i>Input Seed Laser</i>	
Power [MW]	100
Wavelength [nm]	240 - 300
Waist size [microns]	300
<i>Input Electron Beam</i>	
Energy [GeV]	1.2
Current [A]	800
Rms energy spread [keV]	150
Rms emittance [mm-mrad]	1.5
<i>Modulator Undulator</i>	
Period [m]	0.16
Length [m]	3.04
Number of periods	19
<i>Radiator Undulator</i>	
Period [m]	0.065
Section length [m]	2.34
End drift length [m]	1.04
Number of sections	6
Total length [m]	20.28
FEL parameter ρ	2.9×10^{-3}

As most user proposals for FEL-1 concern ultra-fast, pump-probe and other time-domain phenomena, the relevant electron beam characteristics are those of the “medium bunch” option for which the main body current is ~ 800 A; the flat-top duration is ~ 700 fs (which allows for timing jitter); the total charge is ~ 0.7 nC, and the incoherent energy spread is 150 keV. For FEL-1, the output power is relatively insensitive to the actual value of the energy spread so long as the input laser power and modulator

length can produce a coherent energy modulation ΔE an order of magnitude greater than σ_E . A nominal laser power of 100 MW has been adopted; lower values would require increasing the modulator length beyond the ~ 3 m used here. The laser beam comes to a focus halfway in the modulator with a rms waist size of $300 \mu\text{m}$. This value is significantly greater than the electron beam transverse size so as to minimize the induced incoherent energy spread.

Figure 4.4.1 shows the undulator layout for FEL-1 that includes a modulator, dispersive chicane, and the radiator sections consisting of active undulators and end drifts.

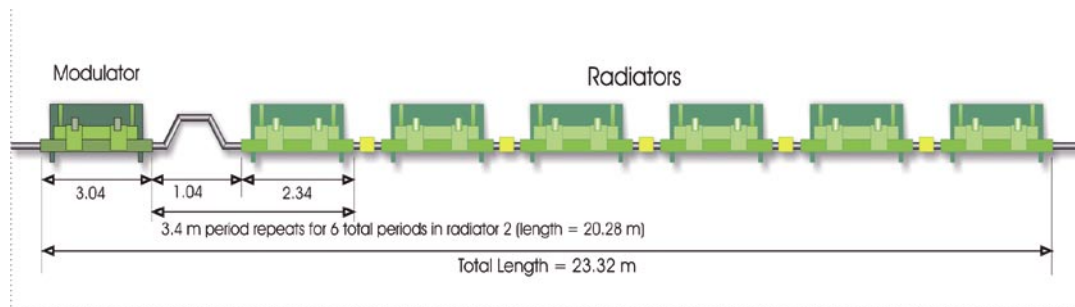


Figure 4.4.1:

Nominal undulator layout for FEL-1. The radiator consists of 6 sections, each 2.34 m long separated by 1.04 m drifts containing a focusing quadrupole, phase corrector, and diagnostics.

Between the modulator and radiator is a dispersive section whose purpose is to convert energy modulation into strong microbunching.

The electron beam and seed laser enter from the left. The drift length between the modulator exit and radiator entrance, and between the individual radiator sections, is 1.04 m including the space associated with the partial strength poles at entrance and exit. At the modulator exit, the peak-to-peak energy modulation, $2\Delta E$, is ~ 4 MV and the rms energy spread is ~ 1 MV. A simple scaling argument ($R_{56} \times \Delta E/E = \lambda_{\text{MOD}}/4$) suggests that the necessary R_{56} is about 35 microns, close to the design value.

For purposes of FEL gain simulations, each radiator undulator section is 2.34-m long and is composed 16 full-strength 6.5 cm periods. Two periods or fewer are required for adiabatic transition to and from each end drift, resulting in a physically usable drift section length of 0.84 m. In the calculations, each drift section includes a “perfect” phase shifter that ensures the longitudinal phase slippage in the drift is an exact multiple of 2π . Since photon number is a critical parameter for FEL-1, the nominal layout includes sufficient sections (6) in the final radiator to ensure power saturation at the shortest design wavelength (40 nm), although as few as three sections are necessary for saturation at 100-nm wavelength.

The general procedure for optimizing the undulator parameters for each wavelength was as follows. The normalized modulator strength a_w ($= K/\sqrt{2}$ for a linearly-polarized undulator) was set to the nominal FEL resonance value. Then the radiator performance was optimized with respect to values of the dispersion parameter R_{56} and a_w . Figure 4.4.2 displays the growth of power and coherent microbunching at 40-, 60-, and 100-nm wavelengths as predicted by the GENESIS and GINGER codes for the parameters of Table 4.4.1.

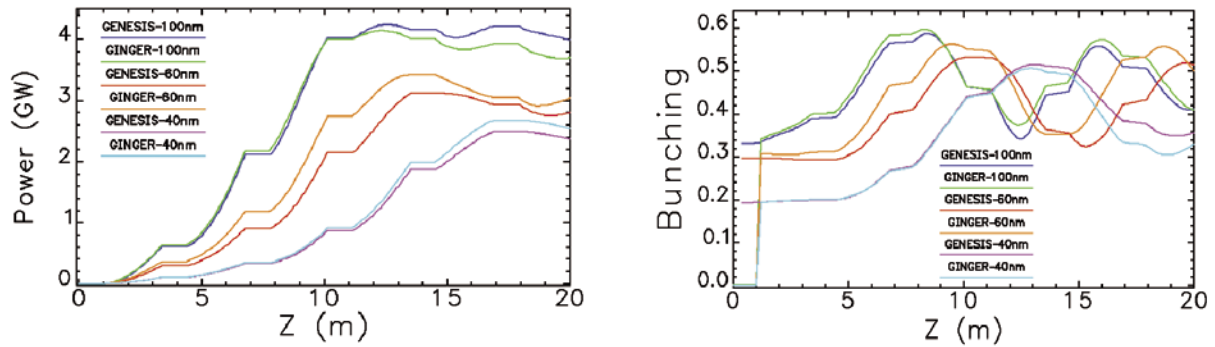


Figure 4.4.2:
GENESIS and GINGER results for radiation power and microbunching fraction for FEL-1 at 100-, 60-, and 40-nm wavelengths.

At the longer wavelengths power and bunching saturation was reached well before the end of the sixth section. The figure also shows good basic agreement between the GENESIS and GINGER predictions. The peak power of 2.5 GW at 40 nm corresponds to an extraction efficiency of 0.26%, quite close to the 3D FEL parameter of 2.9×10^{-3} . That parameter is likely to be an overestimate because the Ming Xie fitting formula [6] does not allow for the 1-m drift sections. The output power can be doubled by properly tapering the six radiator segments.

4.4.1 Sensitivity to Jitter of Input Parameters: Time-Independent Simulation Results

To estimate the sensitivity of output power to electron beam and laser parameters, extensive GENESIS and GINGER simulations were performed varying parameters one at a time. The studies described in this section are limited to axisymmetric effects for both the electron beam and input laser. Section 4.4.2 discusses sensitivity to non-axisymmetric effects such as an input transverse offset or tilt of the entering electron beam. Each individual beam or seed parameter was varied around a central value for the “medium bunch” case, as shown in Table 4.4.1. The calculations were done in the “time-independent” or “time-steady” limit in which all properties of a time-varying electron and laser pulse are replaced by a single, representative value. This approximation models performance with just a single longitudinal “slice,” thus dramatically reducing computational time. To estimate the expected shot-to-shot jitter in the output power and photon number of FEL-1 at 40 nm (i.e., the wavelength with the greatest sensitivity), time-independent calculations were performed in which the input laser seed power and various electron beam quantities were varied independently around their individual design values following a tolerance budget summarized in Table 4.4.2.

Two sets of calculations were done for FEL-1. First, fluctuations of only a single parameter were considered. For each electron beam parameter (*e.g.*, energy, current, *etc.*), a Gaussian distribution of 50 parameter values was generated with the appropriate standard deviation (Table 4.4.2).

Table 4.4.2: Adopted Shot-to-Shot Variation Budget.

<i>Parameter</i>	<i>Normalized shot-to-shot variation</i>
Emittance	10%
Peak current	8%
Mean energy	0.10%
Energy spread	10%
Seed power	5%

Each value was used in different GINGER simulation runs to initialize the electron beam (or input seed laser). Then, a second set of calculations was done with simultaneous, multi-parameter jitters; a set of 400 parameter values were created in which each and every beam parameter was randomly varied following the appropriate Gaussian distribution. These runs produced the data for the curves of Figure 4.4.3, where, as an example, only sensitivity to energy and current fluctuations are reported.

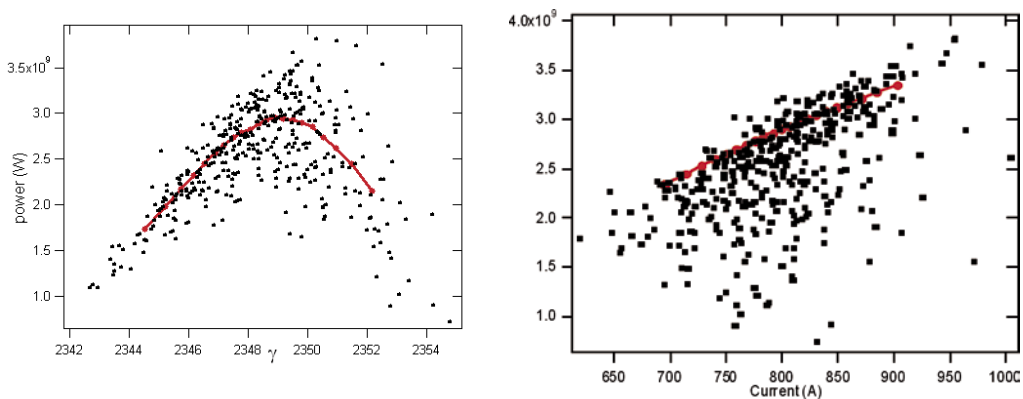


Figure 4.4.3:

Left: FEL output power as a function of electron beam energy in the case of a single parameter only (curve) and multiparameter (dots) variation.

Right: FEL output power as a function of beam current in the case of a single parameter only (curve) and multiparameter (dots) variation.

First, the effect of a jitter only in the mean electron energy was considered based on a Gaussian distribution with a normalized rms of 0.1% – the design goal for beam energy at the end of the linac (see Chapter 6). The single parameter sensitivity scans show that energy plays a crucial role in the FEL performance of FERMI. The multiparameter results (see Figure 4.4.3 left) of output power vs. beam energy, although they show scatter due to the other parameters fluctuations, remain very well correlated to the electron energy variation.

For the case of current jitter (see Figure 4.4.3 right), the output power grows monotonically with increasing current. As was true for the electron beam energy, one sees a clear correlation between multi-parameter jitter output power and the input electron beam current. For the adopted central design point, FEL-1 shows little sensitivity to the electron beam incoherent energy spread, emittance and seed laser power (data not shown). The overall (multi-parameter) estimated fluctuation in output power is about 22%.

One possible way to reduce the sensitivity of the FEL-1 output power to the mean electron energy is to enlarge the effective energy bandwidth of the radiator by using different a_w values in different undulator sections of the radiator. With this approach, electron bunches with mean energies slightly different from the nominal value will still encounter some section whose a_w is close to FEL resonance. To reduce sensitivity to the mean electron energy without simultaneously increasing sensitivity to electron beam current, a simple tapering configuration was investigated. Section by section, a_w was alternatively set to higher and lower values relative to a constant tapering along z . To lowest order, this type of variation favors neither higher nor lower beam energies (relative to the nominal value). For this new configuration the normalized standard deviation of the output power for the adopted energy jitter is less than 5%, and, more importantly, the power fluctuations are also reduced in the multi-parameter jitter case down to about 10%.

4.4.2 Input Transverse Tilt and Offset Sensitivity

Control of displacements and tilts of the electron beam is important to insure the performance of the FERMI FEL. Electron beam offsets can occur due to upstream pointing errors, undulator misalignments, or internal structure in the electron bunch arising from time-dependent linac wakefields, in which case they will also be sensitive to timing jitter. FEL performance in the presence of such offsets was modeled with the GENESIS code, because a fully three-dimensional field solver is necessary to capture all non-axisymmetric effects. Simulation studies included initial offsets for the electron beam only; the laser seed and undulators were assumed to lie along a common axis.

“Global” sensitivity studies simulating various types of jitter simultaneously – including jitter arising from initial tilt or offset – were performed at various wavelengths. The most prominent effect of electron beam offsets is a large drop in output power when the transverse overlap in the first undulator between the electron beam and input radiation seed decreases significantly. In addition, the FEL radiation beam develops offsets comparable to those of the electron beam. Investigation of the behavior of the output phase revealed that phase variations with longitudinal position can significantly affect the spectral width of the output radiation. As was true for the jitter studies without offsets or tilts, the most significant source of shot-to-shot fluctuations is predicted to be jitter in the electron beam energy. However, when using expected values for fluctuations in the electron beam and laser seed power, simulations suggest that the combined effect of the jitter on the other FEL parameters are comparable in some cases to the effect of energy jitter. For the standard deviations chosen, i.e., 100 microns in position and 10 microradians in tilt, the predicted fluctuations in output power for untapered undulators (normalized standard deviations) are 13% at 100 nm, 24% at 60 nm, and 28% at 40 nm. Results for the 40-nm case are shown in Figure 4.4.4.

The output power from tapered undulators shows less sensitivity to jitter in the electron beam energy. Our studies also reveal correlations between beam parameter errors and output power. In addition to mistuning of a_w such that the nominal energy does not quite yield the optimal power (easily corrected

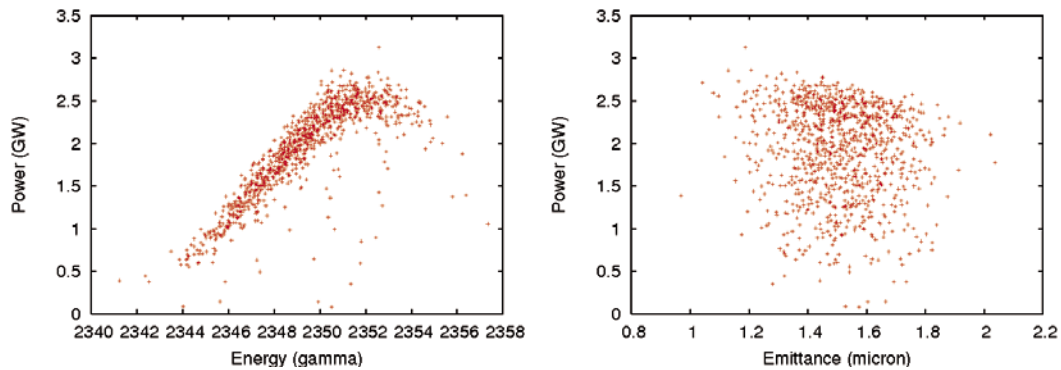


Figure 4.4.4:

Left: Output power versus energy at 40 nm with all input e-beam parameters and the laser seed power simultaneously varying as given in Table 4.4.2. Right: Output power versus emittance.

in practice), the only significant correlation is between the beam transverse emittance and the output power. Rather than reaching a local maximum at the nominal electron emittance, the performance improves significantly as emittance is decreased. The time-dependent jitter study discussed in Section 4.4.3.2 does include such correlations.

4.4.3 Time-Dependent Calculations

Complete “start-to-end” (S2E) simulations that begin at the emitting cathode and end at the undulator exit (for the electron beam) and/or the experimental sample (for the photons) are the most accurate means of estimating the performance sensitivity of an FEL. Extensive modelling of the injector and linac (see chapter 5) yielded so-called “golden” macroparticle files for input in the FEL simulations. Due to the relatively large temporal jitter (~ 350 fs) expected at the linac exit, a pulse shorter than 700 fs FWHM would lead to unacceptable (for use in pump-probe experiments) shot-to-shot fluctuations in output power as many seed pulses would fall temporally outside the electron beam pulse.

Both the GINGER and GENESIS FEL simulation codes were used to predict the full, time-dependent radiation output corresponding to these macroparticle “golden” files. In general, the FEL codes use a total number of macroparticles per time interval that is greater than that generally available from most ELEGANT output files. GENESIS solves this problem by using a special algorithm that creates, as needed, new macroparticles in the “empty” regions of 6D phase space between the ELEGANT macroparticles. GINGER uses a different algorithm with which to populate fully a given time slice; ELEGANT macroparticles from adjacent temporal regions are used with their 5D coordinates (x, x', y, y', γ) carefully interpolated in order to maintain their individual deviation from a coarse-grained average in time. In principle, both algorithms should maintain the local time-dependence of various higher order correlations (e.g., $\langle xy' \rangle$, $\langle \gamma x' \rangle$, etc.).

For both codes, it was necessary to rematch the 4D phase space (x, x', y, y') to the FEL-1 undulator lattice. In FEL operation, rematch will be done by a series of dipoles and quadrupoles upstream of the

modulating undulator. Computationally the rematching was accomplished by determining the Twiss α and β in the central temporal regions of the ELEGANT files, computing the requisite transformation matrix to give the correct match, and then applying this matrix to all the macroparticles. This calculation uses only the temporally-central, “well-behaved” portion of the electron beam thereby neglecting any current spikes the head and/or tail regions with “abnormal” phase space properties.

Nearly all the FEL-1 time-dependent simulations were done at 40 nm for which FEL performance is most critical. The input radiation seed was taken to be either a Gaussian temporal profile pulse of 100 fs (FWHM) – appropriate for pump-probe experiments – or a constant intensity, flat-top pulse in which the laser fully covered the e-beam – appropriate for experiments in which maximum photon number but not timing synchronization is needed.

In all cases the seed beam has a Gaussian transverse intensity profile with a 210-micron waist occurring at the mid-point of the modulator. The simulations normally adopt a temporal slice spacing of either 0.8 fs (i.e., 240 nm) or 1.6 fs. After each modulator run, the particles are rewritten out to disk. They are then read into the subsequent radiator run with the longitudinal phases (relative to a plane wave) multiplied by the harmonic upshift number, in this case 6 (= 240 nm/40 nm). However, the temporal spacing and resolution in the radiator runs remain the same (i.e., 0.8 fs). In other words, the macroparticles are not reorganized into independent 40-nm slices; rather, physical quantities such as current and microbunching fraction at 40-nm wavelength are effectively averaged over a 240-nm interval. So long as the normalized output spectral bandpass is small compared with $40 \text{ nm} / 240 \text{ nm} = 1/6$, this temporal resolution is more than adequate.

4.4.3.1 Expected Performance for the Nominal Working Point

A campaign of time-dependent start-to-end simulations was performed making use of various electron beam distributions provided appropriate to the gun and linac operation (see Chapter 6). Figure 4.4.5 shows the GENESIS-predicted output temporal and spectrum profiles at 40-nm wavelength for an optimized (i.e., flat in both energy and current) input electron beam distribution. The input seed was a 40-fs (rms) Gaussian at a peak power of 100 MW.

The output number of photons per pulse is about 1014 with ~80% in single transverse mode. The output pulse length is 54 fs rms and the relative spectral bandwidth 0.03%, about a factor of 2.2 above the transform limit

As reported in Chapter 6, wakefields arise from the interaction of the electromagnetic fields of the electron beam with the features of the vacuum chamber walls including breaks in the geometry of the

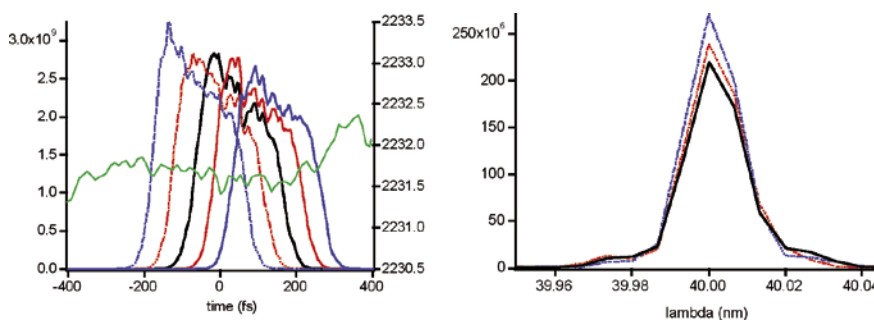


Figure 4.4.5: Left: FEL-1 temporal profiles corresponding to different seed positions along the bunch (green trace, right vertical scale) resulting from a GINGER simulation in time-dependent mode (40 nm). Right: corresponding spectrum profiles.

beam pipe cross-section. Preliminary calculations were performed using a wakefield code based on a numerical physics package developed by H.-D. Nuhn at SLAC. This code currently includes effects from vacuum chamber resistivity, surface roughness, geometric breaks, and a “synchronous term.” Calculations for FERMI assumed a high-aspect ratio, rectangular, Al vacuum pipe of 6.0-mm inner vertical height with a surface roughness of 100-nm amplitude with a longitudinal period of 25 microns. The geometric wake was calculated presuming a 10-cm break occurring every 3.4 meters. An “AC” conductivity model was used for the resistive wake.

With these choices, the resulting longitudinal wakefield is unlikely to degrade FEL-1 output. Apart from large spikes at the head and the tail of ~ 60 kV/m amplitude, the wakes of the particle distribution (see Figure 4.4.6) have temporal variations of only 5 KV/m or less. As shown in Figure 4.4.6, a representative calculation of FEL output with and without wakefield effects included substantiates this assessment.

During the engineering design of the FERMI undulator and vacuum chamber, these wake calculations will be repeated to include more realistic roughness numbers and perhaps a non-circular geometry.

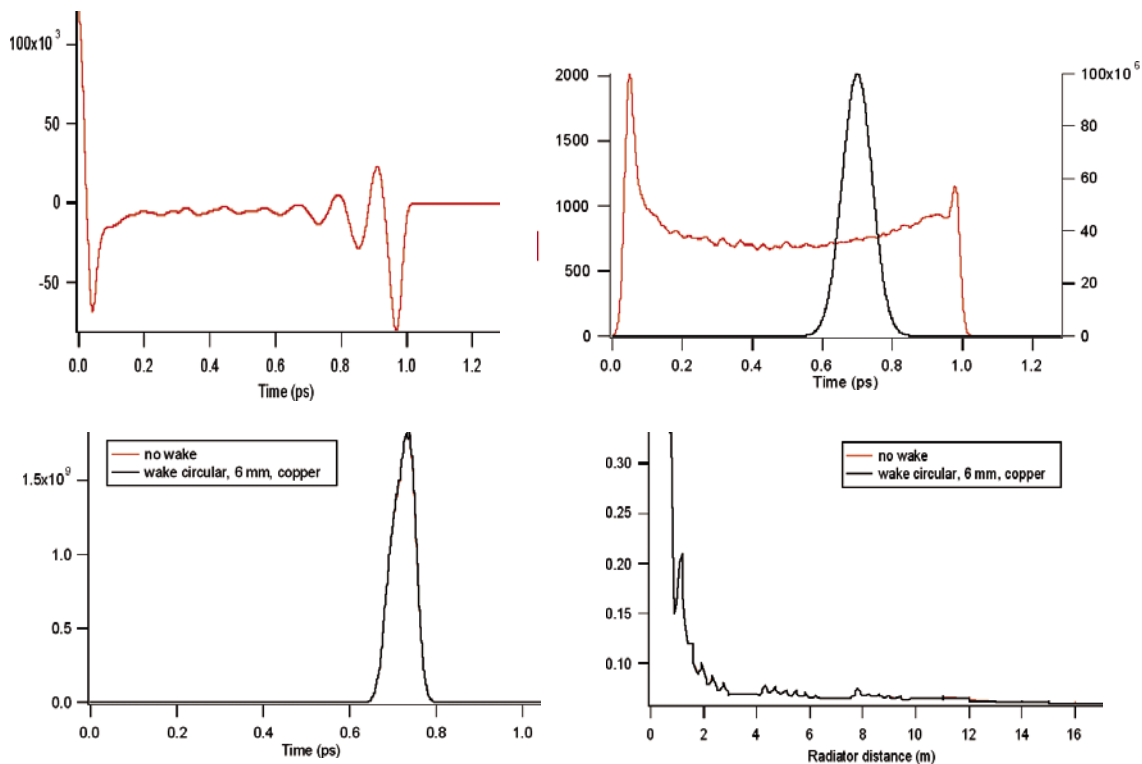


Figure 4.4.6:

Upper left: time-dependent longitudinal wake results for the “medium bunch” distribution (copper, circular cross section with diameter of 6 mm). Upper right: “medium bunch” current distribution (red curve) and temporal

profile of superimposed seed pulse. Down left: temporal profile of the FEL-1 output power resulting from a Genesis simulation including (black curve) and neglecting (red curve) wake fields. Note that curves are practically

overlapped. Down right: Bandwidth as a function of radiator distance (FEL-1) including (black curve) and neglecting (red curve) wake fields.

4.4.3.2 Sensitivity to Jitter of Input Parameters

To examine the effects of injector and accelerator jitters upon the shot-to-shot, time-resolved properties of the output FEL-1 radiation, 100 individual files of 1M macroparticles were propagated starting from the injector (GPT code) through the linac (Elegant code). Each file included the effects of random jitter in the individual injector and accelerator cell voltages. The jitter follows Gaussian distributions with variances set by the budget allowances allocated by the gun and linac groups. GINGER time-dependent simulations for the FEL-1 lattice tuned at 40 nm were performed over a large time window with high resolution. For each jittered file, simulations were done using artificial macroparticles created from the time-dependent envelope quantities previously determined by the *elegant2genesis* code and also using directly the ELEGANT particles. Note that only the effect of the jitter on the electron bunches has been considered without taking into account any jitter source in the seed laser.

The 100 jittered files have been produced starting from one hundred GPT files that consider the possible jitter sources in the gun. Those files have been propagated through the linac with ELEGANT. Output distributions have been pre-processed in order to evaluate the resulting jitter in bunch arrival times (Figure 4.4.7).

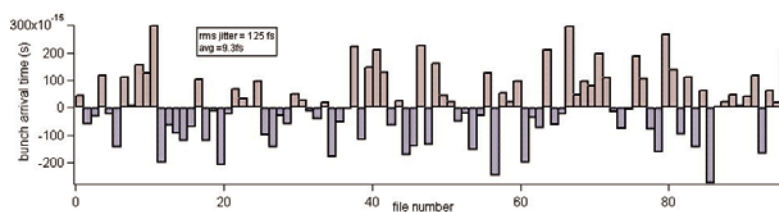


Figure 4.4.7:
Arrival time jitter of the 100 elegant files with respect to the arrival time of the nominal file.

The analysis shows a distribution with an rms jitter of about 130 fs, which is close to the value predicted by LiTrack simulations (see Chapter 6). These data can be fit with a Gaussian distribution (Figure 4.4.8).

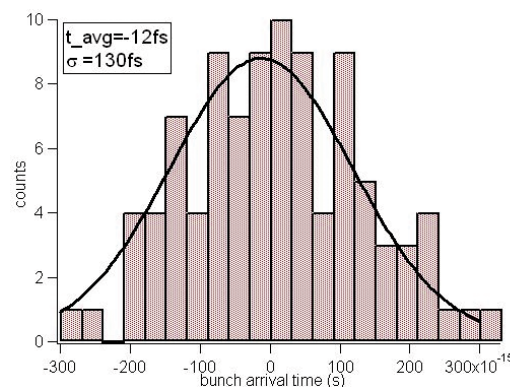


Figure 4.4.8:
Distribution of the arrival time jitter reported in Figure 4.4.7; data can be fitted with a Gaussian distribution, whose sigma is about 130 fs.

By plotting the electron energy and current profiles of the 100 bunches taking into account of the arrival time (Figures. 4.10-4.14) it is evident that a time window exists of the order of 400 fs in which the fluctuations of electron parameters due to the jitter arrival time are small. This window forms the “useful” part of the bunches for the FEL process. The analysis of the effect of variations in electron beam properties on that window is reported in the following.

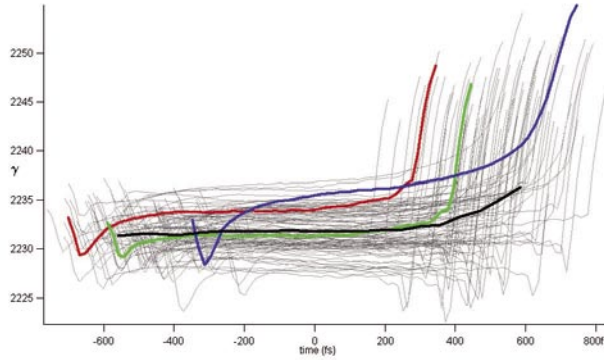


Figure 4.4.9:
Temporal profile of the electron beam mean energy of the one hundred jittered ELEGANT files.

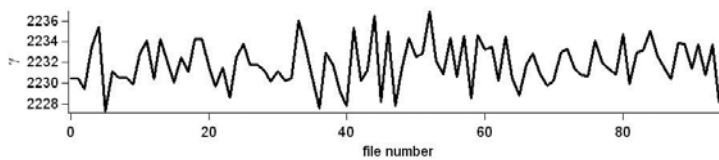


Figure 4.4.10:
Average of the electron mean energy of the jittered electron bunch calculated in the useful time window (-200 fs; 200 fs).

The electron mean energy, γ , in the useful part of the bunch (from -200 fs to 200 fs) presents a distribution with an rms of 0.09%, in agreement with the values of reported in Chapter 6.

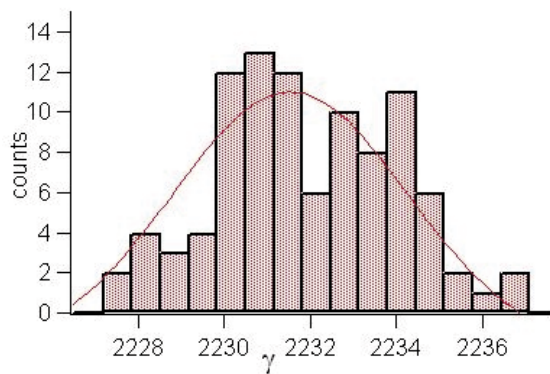


Figure 4.4.11:
Distribution of the average electron mean energy of the useful part of the jittered bunches; data can be fitted with a Gaussian distribution whose sigma is 0.09%.

The current distribution shows an rms value (6.6%) that is slightly lower than the one reported in Chapter 6 (8%). Similar analyses have been performed for other electron beam properties, (emittance, energy spread, etc.). With respect to beam emittance, data show a distribution with an rms value that is close to the one reported in chapter 6 (about 12%). The energy spread, instead, is slightly affected by the temporal jitter of bunches and the rms distribution shows a larger value (almost 20% instead of 10%). Calculated electron beam average values and corresponding standard deviations are reported in Table 4.4.3.

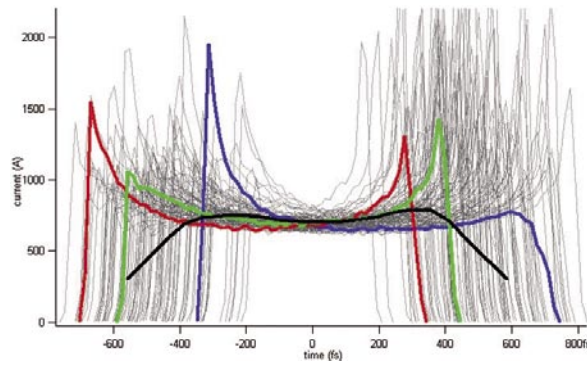


Figure 4.4.12:
Temporal profile for current of the one hundred jittered files.

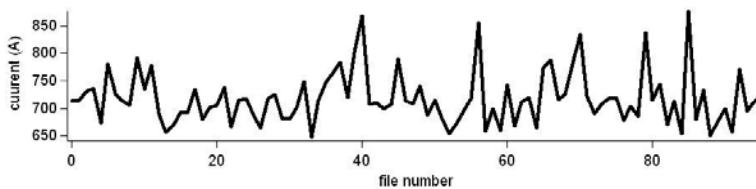


Figure 4.4.13:
Average of the electron bunch current calculated on the useful part of the jittered files (from -200 fs to 200 fs).

Table 4.4.3: Average values and corresponding standard deviations for the main electron beam parameters extracted from time-dependent simulations.

<i>Quantity</i>	<i>Mean Value</i>	<i>Std. Dev.</i>
Gamma	2231.9	0.09%
Current (A)	718	6.6%
Incoherent energy spread	0.33	19.5%
Normalized emittance	1.35	12.4%

The FEL simulations assume the nominal setup of FEL-1 (see Section 4.4) optimized in terms of a_w and R_{56} to maximize the output power extracted from an ideal bunch, whose parameters are equal to the average values reported in Table 4.4.3. Time-dependent simulations using this optimized setup for the jittered files show a high sensitivity to beam jitters (e.g., about 50% of fluctuation in the output power), far from the predictions of time-independent simulations.

Consequently, a new optimization procedure was needed to find baseline characteristics that minimize the effect of the beam jitters. To reduce the sensitivity of the FEL output power the tuning of the radiator was changed slightly to a setting with a smaller value of a_w . The setup utilized for simulations is the following: a seed laser of 100 MW with a Gaussian temporal profile (100 fs rms), the modulator tuned at 240 nm, the dispersive section set with a $R_{56}=19\cdot 10^{-6}$ and the radiator tuned at 40 nm.

Figure 4.4.14 displays the output power profiles obtained from the 100 jitter bunches, while Figure 4.4.16 shows the corresponding output spectra. Red, Green and Blue traces in Figure 4.4.14 and Figure 4.4.16 correspond to the electron bunches reported in Red, Green, Blue in Figure 4.4.9 and Figure 4.4.12.

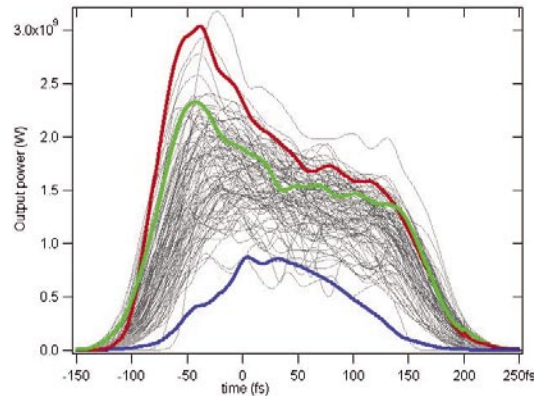


Figure 4.4.14:

Temporal profiles for the FEL output radiation at 40 nm obtained from GINGER simulations using the jittered ELEGANT files; Red, Green and Blue curve refer to bunches reported with the same colors in Figure 4.4.9 and Figure 4.4.12.

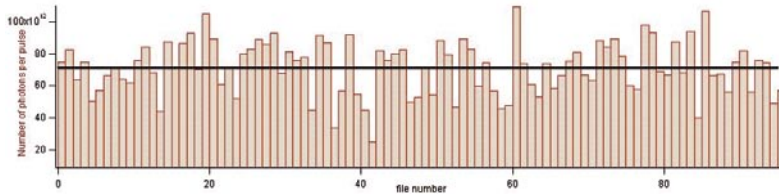


Figure 4.4.15:

Number of photons per pulse obtained from the FEL simulation at 40 nm. Data show an average number of photons of the order of $70\cdot 10^{12}$ with an rms fluctuation of about 23%.

Integrating the pulse profile yields the number of photons of each FEL pulse. Figure 4.4.15 reports the number of photons of FEL output pulses for each of the one hundred jittered electron bunches. Statistical analysis of data shows a distribution that is close to a Gaussian centered at $70\cdot 10^{12}$ photons per pulse with a standard deviation of about 23%.

The output spectra of the FEL pulses shown in Figure 4.4.16 demonstrate that the jitter of the input electron beam parameters induces a fluctuation of the central wavelength. However, such a fluctuation is about a factor 3 smaller than the average bandwidth and, as a consequence, does not affect substantially the FEL

performance (see Table 4.4.4). Considering the equation for the undulator resonance $\lambda = L_w \cdot \frac{(1 + a_w)}{2\gamma^2}$

one can derive that, if the emission wavelength is defined by the resonance wavelength of the radiator, the jitter in wavelength should be two times that associated to the jitter in electron mean energy. This estimate is not true for a seeded FEL in which the emission wavelength is defined by the seeding laser and only partially by the undulator resonance wavelength.

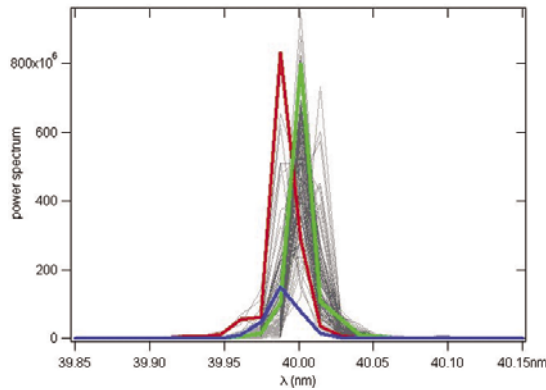


Figure 4.4.16:
Output power spectra obtained from the FEL simulations of the jittered files.

These results are in agreement with predictions and the calculated fluctuation for the wavelength is small compared to the fluctuation of the mean energy of the input jittered bunches.

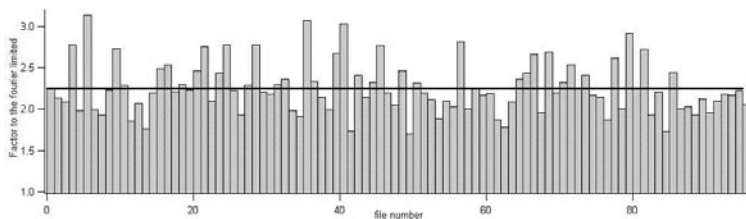


Figure 4.4.17:
Factor to the Fourier transform limit of the FEL output pulses for the jittered ELEGANT files.

The FEL output pulses were also characterized in terms of how close they are to the Fourier transform limit. Figure 4.4.17 shows the distance of each FEL output pulse to the Fourier limit for the one hundred simulated jittered files. The average Fourier factor for the simulated data is 2.2 and the standard deviation of the distribution is about 13%.

Table 4.4.4: Statistics of the one hundred FEL pulses.

Quantity	Mean Value	Std. Dev.
Average pulse width (fs)	73.2	
Average photon number	7.1e+13	23.3%
Average central wavelength (nm)	40.0019	0.013%
Average bandwidth	0.033%	
Fourier factor	2.2	13%

To verify the prediction of time independent simulations that indicate that the jitter in the mean electron energy is the strongest limiting factor for achieving a good output stability, one plots (in Figure 4.4.18) the number of photons per pulse v. the average electron beam energy. The clear correlation between the two quantities confirms the high sensitivity of the FEL output to the mean electron energy.

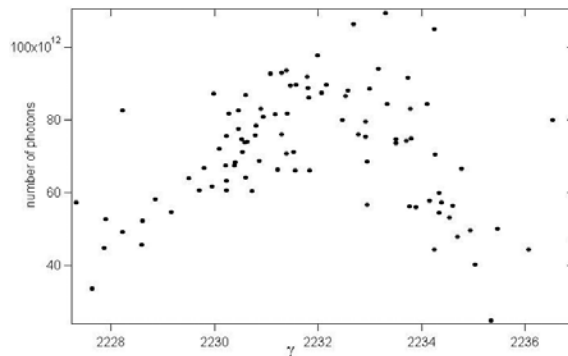


Figure 4.4.18:
Number of photons per pulse v. the average electron mean energy of the corresponding electron bunch.

4.4.4 Diagnostics Needs for FEL-1

Some routine measurements will guide the operators in maximizing the output from FEL-1. Within the different segments of undulator and other lattice elements, electron beam position monitors are needed to ensure that the beam orbit stays as close as possible to the magnetic axis. Following the chromatic dispersion element, the electron bunch will have both strong energy modulation and micro-bunching; the latter can be measured with coherent optical transition radiation (COTR) from an insertable foil. In the radiator, the build up of the coherent harmonic signal can be determined section-by-section by purposely mistuning the magnetic strength of the downstream undulator sections so as to eliminate any additional emission. COTR in the drift sections can also be used to measure the z-dependent evolution of the micro-bunching. The COTR signal should also be rich in harmonics of the initial seed laser. Ideally for comparison with simulations, measurements of the microbunching and FEL radiation should be done following each radiator undulator section. Finally, measurements of the final energy spread of the e-beam upon exit from the final undulator section should be commensurate with the FEL emission from the radiator.

4.5 FEL-2 Design and Parameters Calculations

As mentioned in the Section 4.1, most proposed experiments using FEL-2 will be in the frequency domain, in which case narrow spectral bandwidth is crucial. Consequently, the baseline design of FEL-2 utilizes a relatively long (~ 1.5 ps) electron beam pulse with a moderate (~ 500 A) current. Figure 4.5.1 shows the layout adopted for the fresh bunch approach.

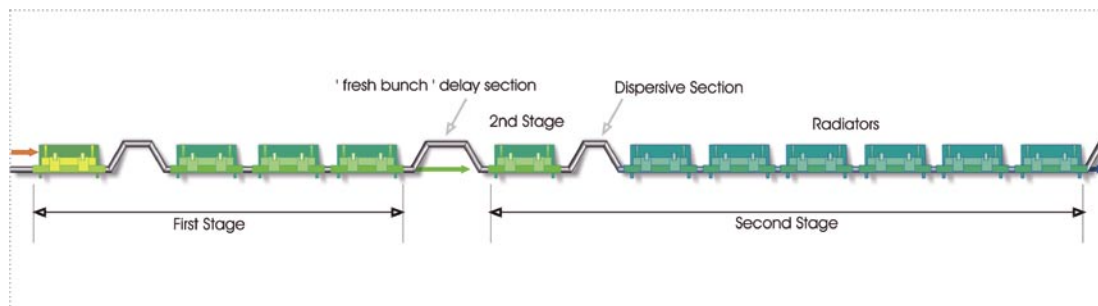


Figure 4.5.1:
Nominal undulator layout for FEL-2.

For the fresh bunch approach, such a long pulse is essential given the practicalities of temporal jitter and the accuracies of a temporal delay section. The core design for the first stage of the fresh-bunch FEL-2 is parallels that of FEL-1. Specifically, relatively strong, input seed power (~ 100 MW) energy-modulates a 500 A electron beam in a long period (~ 16 -cm wavelength) undulator followed by a dispersive section with $R_{56} \sim 25$ μm . The dispersive section produces strong bunching at the fundamental ($b \geq 0.5$) and also at the second through sixth harmonics in the following radiator. Where the design for the FEL-2 fresh-bunch layout begins to differ significantly is that the first stage radiator is relatively short (*e.g.*, 2-3 segments) and only brings the radiation to a sufficient level (~ 200 MW) to provide adequate coherent energy modulation in the following undulator. This choice contrasts with the FEL-1 radiator that is long enough (*e.g.*, 5-6 segments) to reach FEL power saturation (~ 1 -4 GW). The basic characteristics for the second stage modulator are the same as for the first stage radiator (*e.g.*, 65 mm period; 2.34 m segment length) so as to minimize costs. In general, the first stage should be as short as possible to minimize SASE that increases the incoherent energy spread of the “fresh” portion of the e-beam to be used in the second stage modulator and radiator. A secondary consideration is that the cost is also lowered. Provisionally the fresh bunch delay section is presumed to have a 1.8 m length (necessary in the numerical simulations to include proper diffraction effects).

The second stage (final) radiator has a somewhat shorter period (*i.e.*, 50 mm) and is subdivided into 2 m long active segments of undulator separated by 1 m drifts. These breaks contain a quadrupole singlet for focusing, a phase shifter, dipole correctors, and diagnostics. The length of the final radiator is somewhat arbitrary; in general for the fresh bunch approach one wants sufficient length for power saturation, ~ 6 segments at 10 nm wavelength. However, one could certainly increase the output power by adding more radiator segments with tapered magnetic strengths.

4.5.1 Fresh Bunch Time-Independent Results

Following similar strategies described in Section 4.4.1, a series of simulations were performed to optimize the output power of the second stage. As the final design of FEL-2 will be modified based on FEL-1 performance the calculations presented here are representative rather than fully consistent design sets. Assuming that most of the first stage of FEL-2 would be similar to that of FEL-1, the most sensitive quantities to vary are the number of radiator sections in the first stage and the strength of the dispersive section following the second stage modulator. A good design point was a three-section first radiator that would emit ~ 250 MW of power at 40 nm wavelength. With that choice, at the end of the second modulator, the peak-to-peak energy modulation is ~ 1.8 MeV, as compared with 2.5 MeV modulation in the first stage. The final radiator is 6 sections long and produces (see Figure 4.5.2) a peak power of 0.63 GW (1.4 GW) and a bunching of 0.44 (0.53) at 10 nm (20 nm) for 500 A beam current.

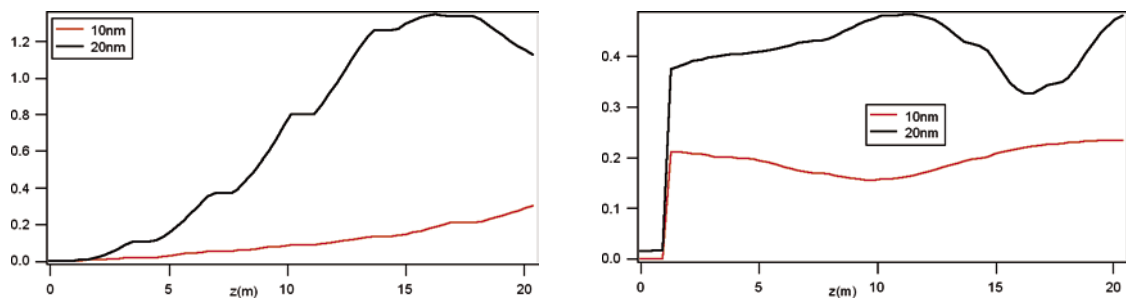


Figure 4.5.2:
Power and bunching for different FEL-2 configurations as a function of position within the radiator.

A small number of time-independent, single parameter variation scans were performed to determine the sensitivity of the final output. Not surprisingly given the much larger total number of undulator periods in FEL-2 as compared with FEL-1 plus the additional sensitivity connected with having a second stage of modulation, one observes a much greater dependence upon electron beam parameters, especially beam energy.

4.5.1.1 Fresh Bunch Time-Dependent Results

A number of full start-to-end simulations were done for the fresh bunch approach to FEL-2. Simulations concentrated upon 10 nm output cases as these were likely to be the most sensitive to imperfect electron beam parameters. The first stage radiator output was at 40 nm so the second stage had a 4:1 up-conversion ratio. An example of output temporal and spectrum profiles based on an optimized input electron beam is shown in Figure 4.5.3.

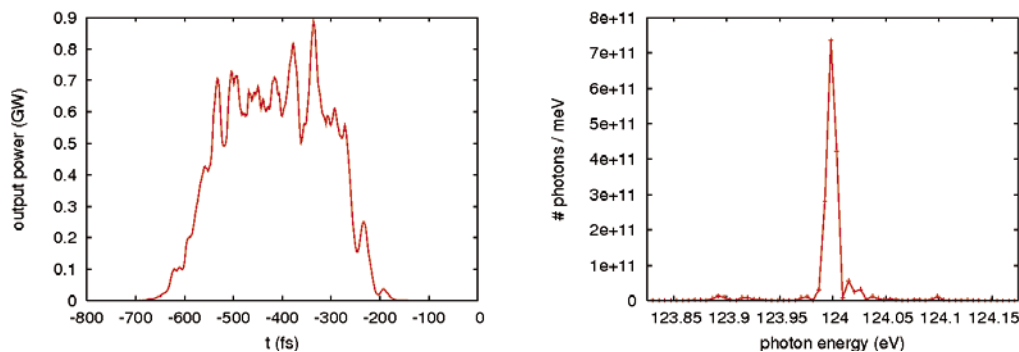


Figure 4.5.3:
FEL-2 temporal and spectrum profiles for fresh-bunch scheme resulting from a GENESIS simulation in time-dependent mode.

The number of photons obtained per pulse is about 10^{13} (93% in single transverse mode). The output pulse length is 110 fs (rms) and the bandwidth 5 meV, about a factor about 1.5 above the transform limit. The peak brightness is about 10^{32} photons / mm²/mrad² / sec / 0.1% bandwidth.

A concern for FEL-2 is whether jitter in beam parameters combined with wakefield effects in the accelerator (discussed at length in Section 6.8.3) will significantly degrade the narrow spectral profile typified by Figure 4.5.3. As displayed in Figure 4.4.16, the fluctuations in beam energy can jitter the position of the peak of the spectrum of FEL-1 by $\sim 10^{-3}$ with little noticeable increase in bandwidth. FEL-2 is more sensitive to jitter in beam parameters than FEL-1 due to the reduced value of ρ in the second radiator. In addition, the amount of bunching produced by the second dispersion section is sensitive to lower input radiation at the beginning of the second stage due to energy mismatches in the first stage of the cascade. Although a detailed quantitative answer to this question would require many hundreds of simulation runs, the analysis the time-variation of energy during the beam pulse given in Section 6.8.3 permits a semi-quantitative answer. These considerations do not include the effect of wakefields in the undulator, discussed in the following section.

For that sub-set of users who require narrow bandwidth radiation, special care will have to be taken to minimize the fluctuations in the non-linear chirp (σ_{a_2} in Eq. 6.8.2) that is induced by wakefields throughout the accelerator and wiggler. As the non-linear (quadratic) component directly influences the radiation bandwidth at the FEL design point, fluctuations in this component could lead to uncertainties in the output bandwidth beyond the few meV level desired by users studying RIXS phenomena. The analysis of Section 6.8.3 indicates that even in the long bunch case the fluctuation in a_2 is $\sim 60\%$, producing a commensurate increase in the effective (average) bandwidth. In the medium bunch case the fluctuation in a_2 is two times smaller, an amount that would not significantly reduce the effective bandwidth. Therefore, in the final design of FEL-2 the pulse length will be selected to optimize the average photon number within the desired 5 meV bandwidth.

The second concern for FEL-2 is whether the fluctuations in the central frequency (which in FEL-2 can be much larger than the bandwidth) are tolerable in RIXS experiments. As RIXS measures only

frequency differences, the jittering of the central value does not matter as long as 1) the output frequency is measured, and 2) the linewidth is sufficiently small.

Even if the quadratic chirp could not be sufficiently well controlled (unlikely in light of the analysis of Section 6.8.3), an alternative approach would be to control the magnitude of the linear component of chirp. Then, unlike the behaviour seen in Figure 4.4.16, the central value of the spectrum would remain fixed by the central value of the spectrum of the seed laser with the bandwidth varying from pulse-to-pulse. One could then use a monochromer upstream of the experimental sample. Options for the placement of this monochromer are presently being studied.

4.5.2 Wakefield Calculations

As was done for the FEL-1 “medium bunch” in Section 4.4.3.1, the expected longitudinal wakes were also calculated in the FEL-2 “long bunch” case. As before, the rectangular Al vacuum chamber characteristics were 6.0 mm vertical inner height, a surface roughness of 100 nm amplitude with a longitudinal period of 25 microns, and a presumed 10 cm break occurring every 3.4 meters. The resistive wake calculation was based upon an AC conductivity model. Figure 4.5.4 shows the calculated wakes versus distance back from the beam head.

Once again, with the exceptions of possible spikes in the head and tail regions, over an interval exceeding 1.0 ps there is a nearly constant wake of ~ 4.4 kV/m with temporal fluctuations of ± 2.5 kV/m or so.

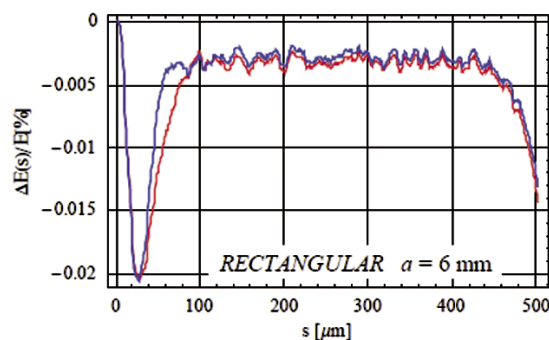


Figure 4.5.4: Time-dependent longitudinal wake results for the “long bunch” distribution. Red corresponds to the aluminum and blue to the copper chamber respectively.

Over a 50 m total vacuum chamber length, a fluctuation of ± 150 kV corresponds to less than 0.01% of total energy – much less than the FEL parameter. Consequently this variation is unlikely to cause any significant degradation of emitted power. Moreover, as the wake function from the wiggler has very little curvature, the wakefield in the wiggler will have minimal effect on the line width of FEL-2.

Fluctuations in power are equivalent to a slight line broadening, but do not shift the output wavelength. In contrast, if the surface roughness were to grow to ~ 500 nm amplitude, the fluctuations from this wake component increase by a factor about 25 to approximately 15 kV/m. Over 40 m of vacuum chamber, this wake would lead to a normalized beam energy fluctuation of 0.05% which could prove quite troublesome both in output level and in bandwidth. Therefore, further studies are needed to set specifications and tolerances for the FEL-2 vacuum chamber as a compromise between ease and cost of fabrication and FEL performance. In any case the conclusions presented at the end of the preceding section remain valid.

4.5.3 Diagnostics Needs for FEL-2

For most items, the diagnostic needs of FEL-1 and FEL-2 are quite similar. The first stage of FEL-2 can be considered a somewhat shorter version of FEL-1 and the various diagnostics proposed for FEL-1 could be replicated here. For the fresh bunch approach, the output radiation of the first stage will be used to modulate a portion of the electron bunch; therefore, detailed radiation diagnostics would prove extremely useful. In order to tune the delay section between the first and second stages, a cross-correlator between the first stage coherent signal and the spontaneous emission from the second stage might be useful. In addition a diagnostic of micro-bunching after the second stage modulator is likely to be essential. A diagnostic to resolve in z the build up of coherent radiation in the second stage radiator would also provide valuable information. Since the undulator gaps can be opened, a gross mistuning downstream of the desired diagnostic point might be sufficient.

4.5.4 Results for the “Alternative” Whole Bunch Configuration and Comparison with Fresh Bunch Approach

An alternative scheme that was considered for FEL-2 is based on the so-called “whole-bunch” approach. Here, the entire electron beam pulse is energy-modulated by the external laser seed and, following the first radiator, there is neither a temporal delay section nor a second modulator. Instead, the electron beam immediately enters a weak dispersive section followed by a second radiator whose FEL resonant wavelength is tuned to an integer harmonic of the first radiator. Due to the relatively small harmonic micro-bunching at this new wavelength, this second radiator must operate deep in the exponential gain regime. Thus, to keep the exponential gain length and power saturation lengths acceptably small, the energy modulation produced by the first (and only) modulator must be relatively small compared to ρ_2 where ρ_2 is the FEL parameter for the second radiator (generally $\sim 1 \times 10^{-3}$).

This small energy modulation means that at entrance to the first radiator the e-beam will have a smaller micro-bunching level relative to that of the fresh bunch scheme. Consequently, the whole bunch approach can fail (in terms of the needed second radiator undulator length for saturation) if the initial energy spread becomes too large. Moreover, because the micro-bunching level is small at the beginnings of both the first and second radiator, the relative strength of the shot noise micro-bunching is much higher and the final SASE strength can be two or more orders of magnitude greater in the whole bunch approach than in the fresh bunch approach. The main potential advantage of the whole bunch scheme is that it is less sensitive to shot-to-shot fluctuations of the relative timing between the e-beam and external seed laser. This advantage comes with the price of great difficulty in producing an electron bunch with minimal non-linear energy chirp.

A representative output temporal profile and spectrum obtained at 10 nm using the whole bunch configuration are shown in Figure 4.5.5. The initial electron beam distribution used is the same as for the fresh-bunch calculation shown in Figure 4.5.3.

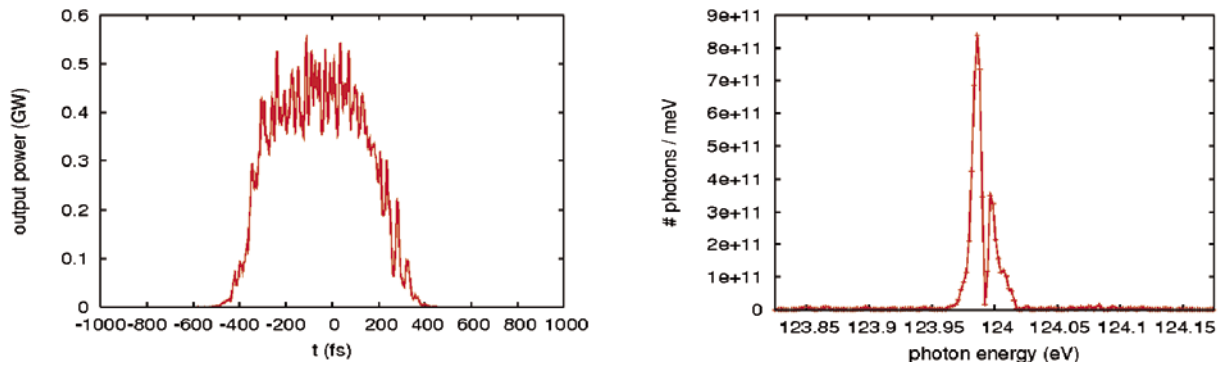


Figure 4.5.5:
FEL-2 temporal and spectrum profiles
for whole-bunch scheme resulting
from a GENESIS simulation in time-
dependent mode.

In this whole-bunch example, the number of photons obtained per pulse is about 10^{13} (93% in single transverse mode). The output pulse length is 200 fs (rms) and the bandwidth 4 meV. This gives a result which is a factor about 2.5 above the transform limit.

4.7 References

- [1] L.H. Yu et al., Phys. Rev. Lett. 86 (2001) 5902.
- [2] A. Doyuran et al., Phys. Rev. Lett. 91 (2003) 07480.
- [3] I. Ben-Zvi, K. M. Yang, and L. H. Yu, Nucl. Inst. Meth. A, 318, (1992) 726.
- [4] S. Reiche, Nucl. Instrum. Meth. A 429 (1999) 243.
- [5] W. Fawley, Report LBNI-49625, 2001.
- [6] Ming Xie, Nucl. Instrum. Meth. A 445, (2000) 59.

Table of Contents

4	FEL Physics	73
4.1	Introduction	74
4.2	Basic FEL Output Requirements and Related Issues	76
4.3	Undulator and Transport Lattice Design	78
4.3.1	Choice of Undulator Type and Wavelength	78
4.3.2	Undulator Segmentation and Focusing Issues	78
4.3.3	Undulator Error Tolerance Calculation	79
4.3.4	Post-Modulator Dispersive Section Design and Issues	81
4.3.5	Delay Section Needs and Issues for FEL-2 Fresh-Bunch Approach	81
4.4	FEL-1 Design and Parameters Calculations	82
4.4.1	Sensitivity to Jitter of Input Parameters: Time-Independent Simulation Results	84
4.4.2	Input Transverse Tilt and Offset Sensitivity	86
4.4.3	Time-Dependent Calculations	87
4.4.4	Diagnostics Needs for FEL-1	95
4.5	FEL-2 Design and Parameters Calculations	96
4.5.1	Fresh Bunch Time-Independent Results	97
4.5.2	Wakefield Calculations	99
4.5.3	Diagnostics Needs for FEL-2	100
4.5.4	Results for the “Alternative” Whole Bunch Configuration and Comparison with Fresh Bunch Approach	100
4.6	References	102